Check for updates

rGO/MnO_2 nanowires for ultrasonic-combined Fenton assisted efficient degradation of Reactive Black 5

Martha Ramesh, Martha Purnachander Rao, F. Rossignol and H. S. Nagaraja

ABSTRACT

Reduced graphene oxide (rGO) coated manganese dioxide (MnO_2) nanowires (NWs) were prepared by the hydrothermal method. Raman spectra confirmed the presence of rGO and the Brunauer–Emmett–Teller surface area of rGO/MnO_2 NWs was found to be 59.1 $m^2 g^{-1}$. The physico-chemical properties of prepared catalysts for the degradation of Reactive Black 5 (RB5) dye were investigated. 84% of RB5 dye in hydrogen peroxide solution was successfully degraded using rGO/MnO_2 NWs, while only 63% was successfully degraded with pristine α-MnO_2 NWs in 60 min owing to the smaller crystallite size and large surface area. Further, the ultrasonic-combined Fenton process significantly enhanced the degradation rate to 95% of RB5 by the catalyst rGO/MnO_2 NWs due to synergistic effects. The decomposition products identified using gas chromatography-mass spectrometry revealed a higher production rate of fragments in the ultrasonic-combined Fenton process. Therefore, rGO/MnO_2 NWs with the ultrasonic-combined Fenton process is an efficient catalyst for the degradation of RB5, and may be used for environmental protection.

Key words | catalysis, MnO_2 NWs, nanowires, rGO, RB5, ultrasonic-combined Fenton

Martha Ramesh (corresponding author)
H. S. Nagaraja
Materials Research Laboratory, Department of Physics,
National Institute of Technology Karnataka,
Surathkal,
Mangalore 575 025,
India
E-mail: *ramesh.martha09@gmail.com*

Martha Purnachander Rao
Nanomaterials and Solar Energy Conversion Laboratory,
Department of Chemistry, National Institute of Technology,
Trichy 620015,
India

F. Rossignol
SPCTS, UMR 6638, ENSCI, CNRS,
Centre Européen de la Céramique,
12 rue Atlantis,
Limoges Cedex 87068,
France

INTRODUCTION

Large amounts of synthetic/reactive dyes including Reactive Blue, Reactive Red and Reactive Yellow, are used in industry for dying and colouring materials. Reactive Black 5 (RB5) dye is much used in textile colouring due to its special features such as solubility, high shade of the colour and easy attachment to fibre (Vijayaraghavan *et al.* 2013). During the colouring/dying process, a significant proportion of dyes are released into the environment which affects aquatic life, drinking water and the health of human beings (Gupta *et al.* 2012; Karatas *et al.* 2012). Hence the removal of organic pollutants from waste water is a major environmental challenge. In this regard, a wide variety of methods, such as biological, physical and chemical methods have been developed to remove RB5 molecules from waste water (Siboni *et al.* 2011; Kalkan *et al.* 2014; Sadeghi *et al.* 2014; Amin *et al.* 2015). All of these approaches have some drawbacks, such as formation of by-products, slow reaction rate for the degradation of RB5 molecules, the need for dissolved oxygen and long retention time, low efficiency, and some of them are very expensive. Therefore, development of a suitable catalyst and a simple, efficient and environmentally friendly method is essential.

Metal oxides (Poulios & Tsachpinis, 1999; Aguedach *et al.* 2008; Kansal *et al.* 2009; Chong *et al.* 2015) have applications as catalysts for the degradation of RB5 owing to their structural and optical properties which play a crucial role in the catalytic activity. Among these, MnO_2 draws much attention due to its relatively low crystallite size and large surface area (Kumar *et al.* 2014). In particular, MnO_2 has revealed a superior catalytic activity and adsorption capability for dye degradation and heavy metal ion removal from wastewater. For instance, single crystalline β-MnO_2 nanowires (NWs) fabricated by a simple hydrothermal method showed a maximum degradation rate of 95% for methylene blue in the presence of hydrogen peroxide (Zhang *et al.* 2015). Up to now, many methods like redox-precipitation (Wu *et al.* 2013), microwave irradiation (Ai *et al.* 2008), and vapor–liquid–solid (Li *et al.* 2005) have been proposed to synthesize nanocrystalline MnO_2. However, these methods suffer from drawbacks such as agglomeration, stability, heat control, pressure issues, requirement of high

doi: 10.2166/wst.2017.291

Downloaded from http://iwaponline.com/wst/article-pdf/76/7/1652/450029/wst076071652.pdf
by guest

temperatures, low reaction rate and production of secondary nanostructures. Recently, a graphene/MnO_2 nanocomposite has proved to have superior electrode performance in super capacitor applications, using graphene oxide and manganese sulphate as the precursors (Feng *et al.* 2013).

The Fenton reaction suffers from the drawback of the constant loss of the catalyst (Zhang *et al.* 2006; Harichandran & Prasad 2016). In this regard, ultra-sonication can be used as a support, during which the propagation of the sound wave through the Fenton reaction causes extremely high temperatures and pressures in a microscopic region of the sonicated liquid, thereby resulting in chemical excitation, resulting in the initiation or enhancement of the catalytic activity in the solution through the formation of new, relatively stable chemical species that can diffuse further into the solution to create chemical effects. Hence, an ultrasonic-combined Fenton reaction in an aqueous solution not only enhances the amount of free radicals, but also alters the reactor conditions favouring a good interaction of the created free radicals with the organic effluents for efficient removal (Namkung *et al.* 2008; Song *et al.* 2009). Recently it has been used in the improvement of degradation of several reactive dyes, such as Rhodamine B (Chen *et al.* 2016), Reactive Blue 181 (Basturk & Karatas 2014) and Reactive Blue 49 (Siddique *et al.* 2014), but the use of an ultrasonic-assisted Fenton reaction for the decoloration of RB5 dye using reduced graphene oxide (rGO)/MnO_2 NWs has not yet been reported.

Herein, we report the synthesis and physico-chemical properties of rGO coated MnO_2 NWs for enhanced catalytic decoloration of RB5 dye with an ultrasonic-combined Fenton process. Further, both rGO coating and ultrasonication of the NWs reveal an increase in decoloration of RB5 by 30%. Also, a higher production rate of organic fragments in the ultrasonic-combined Fenton process is witnessed.

MATERIALS AND METHODS

Graphite powder and RB5 dye were purchased from Sigma-Aldrich and used as received. Manganese sulfate, potassium permanganate, sodium nitrate, sodium hydroxide, sulfuric acid (98%), hydrogen chloride, and hydrogen peroxide (30%) from Merck were used to produce the NWs. All reagents were of analytical grade. The crystalline phases of the products were identified using powder X-ray diffraction (Rigaku miniflex 600, Japan) using CuKα radiation (λ = 1.5406 Å). Scanning electron microscopy (JEOL/JSM-6380LA, Japan) was employed to observe the morphologies and sizes of the NWs. The Raman spectra was registered in the spectral range of 400–2,000 cm^{-1} using a Raman spectrometer LabRam HR800 (Horiba Jobin Yvon Inc. USA). The specific surface area of the prepared samples was estimated using the Brunauer–Emmett–Teller (BET) method from the nitrogen adsorption–desorption isotherms obtained using a BELSORP Mini II instrument (BEL Japan Co., Ltd). The concentration of the RB5 dye after degradation was recorded using a UV-Vis spectrometer (ocean optics USB4000-UV-VIS, India). All reactions were conducted with stirring, using a magnetic stirrer (Remi MLH Plus, India) at 700 rpm and centrifugation was carried out using a centrifuge (Remi, R-8C, India). The aqueous solutions were sonicated using a Le-120UPP (20 KHz, 120 W, Leela Electronics Company, India) sonicator. To evaluate the by-products, gas chromatography-mass spectrometry (GC–MS) was used (GCMS-QP 2010 Plus Shimadzu mass spectrometer). An HP-5 ms column with dimensions of 0.25 μm, 30 m × 0.25 mm (i.d.) was used. The temperature was ramped as follows: 36 °C for 1 min, 5 °C min^{-1} up to 300 °C and hold time 10 min. The temperature of the inlet, source and transfer line was 250, 230 and 280 °C, respectively. The analyses were done using splitless (0.7 min) injection.

Synthesis of rGO

A modified Hummer's method was used to prepare rGO (Sreejesh *et al.* 2015). To prepare graphene oxide, 0.5 g of sodium nitrate, 1 g of graphite flakes and 23 mL of concentrated sulfuric acid, were stirred on a magnetic stirrer at room temperature to form a homogeneous solution. 3 mg of potassium permanganate was added to the above solution within 1 h to avoid the rise of temperature of the mixture and the suspension was continuously stirred at 35 °C for 12 h. Finally, the solution was oxidized by adding 5 mL 30% hydrogen peroxide to the above suspension. To remove the organic residues and other metal ions in the mixture as a result of reduction of potassium permanganate, the brown solid product was centrifuged at 2,000 rpm for 30 min at each time by soaking with deionized water and 5% hydrogen chloride for several times, then dried at 60 °C in a vacuum oven for 12 h. The obtained product was dispersed using ethanol and calcined at 150 °C for 4 h to reduce GO into rGO.

Synthesis of MnO_2 NWs and rGO/MnO_2 NWs

In a typical synthesis, the manganese sulfate was annealed at 500 °C for 3 h to eliminate water content, resulting in the

Downloaded from http://iwaponline.com/wst/article-pdf/76/7/1652/450029/wst076071652.pdf
by guest

formation of anhydrous manganese sulfate. 0.2 M of anhydrous manganese sulfate and 0.63 M of potassium permanganate was taken separately in 30 mL of distilled water. Then the mixture was stirred in a magnetic stirrer at ambient conditions to form the uniform suspension. MnO_2 was obtained from the oxidation of anhydrous manganese sulfate by potassium permanganate using the reaction,

$$2KMnO_4 + 3MnSO_4 + 2H_2O \rightarrow 5MnO_2 + K_2SO_4 + 2H_2SO_4 \quad (1)$$

After 1 h, the viscous liquid was transferred into a 100 mL Teflon-lined stainless steel autoclave and maintained at 150° for 24 h, then cooled down to room temperature. The resulting block solid suspension was washed with distilled water, filtered and dried at 60 °C. In order to transform Mn^{2+} into MnO_2, additional potassium permanganate was added slowly into the system following the stoichiometric reaction equation (Peng *et al.* 2013),

$$2MnO_4^- + 3Mn^{2+} + 2H_2O \rightarrow 5MnO_2 + 4H^+ \quad (2)$$

rGO-MnO_2 NWs were prepared using the same method as described above by adding 0.025 g of rGO to the above solution.

RESULTS AND DISCUSSION

MnO_2 NWs and rGO/MnO_2 NWs were characterized by X-ray diffraction as shown in Figure 1(a). All the diffraction peaks of MnO_2 NWs were indexed and matched well with the body-centered tetragonal phase, with lattice constants a = b = 9.7847 Å and c = 2.8630 Å, which agrees with standard JCPDS No. 44–0141 (Zhong 2016). The appearance of the broad diffraction peak positioned at 23.7° corresponds to the (002) plane, indicating the presence of an rGO on the surface of rGO/MnO_2 NWs. The interlayer spacing of rGO is 0.37 nm, slightly larger than that of graphite, which resulted from the small amount of residual oxygen-containing functional groups or other structural defects (Fu *et al.* 2013). These two samples have apparent variations in the intensity and broadening of the diffraction peaks. As seen in Figure 1(a), with the coating of the rGO, the intensity of MnO_2 NWs peak decreases and peak broadening increases. In the case of bare MnO_2 NWs, the crystallites are larger in size, resulting in a narrow diffraction peak. However, the smaller crystallites of rGO/MnO_2 NWs account for the observed peak broadening. From the diffraction using the high intensity peak (211), the crystallite size of MnO_2 and rGO/MnO_2 was estimated using Scherrer's equation (Zang & Tang 2015),

$$D = \frac{K\lambda}{\beta \mathrm{Cos}\theta} \quad (3)$$

where D is the mean size of the crystallite (nm), K is the shape factor equal to around 0.9, λ is the X-ray wavelength, 0.154 nm of CuK_α radiation, β is the line widening at half intensity of the peak (radians), and θ is the angle of the diffraction peak (degrees). The measured crystallite size of the MnO_2 NWs was in the range 14–23 nm. Further, from

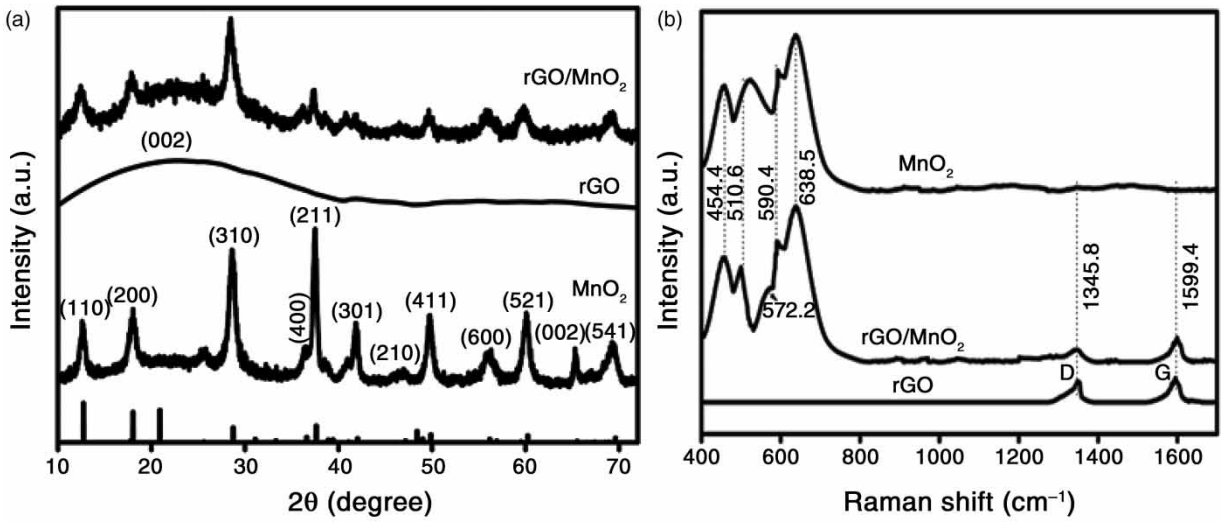

Figure 1 | (a) X ray diffraction and (b) Raman spectra of α-MnO_2 NWs and rGO/MnO_2 NWs.

Downloaded from http://iwaponline.com/wst/article-pdf/76/7/1652/450029/wst076071652.pdf
by guest

Table 1, it can be observed that the average crystallite size of MnO_2 NWs decreases with the coating of the rGO. Using the above crystallite values, the dislocation density (δ), which reveals the amount of defects in a unit volume of MnO_2 and rGO/MnO_2 NWs, was estimated using Williamson and Smallman's formula (Williamson & Smallman 1956),

$$\delta = \frac{1}{D^2} \tag{4}$$

Evidently, rGO/MnO_2 NWs consist of more dislocations due to heterogeneous nucleation, as well as interfaces between the MnO_2 lattice and rGO nanosheets (Abdolhosseinzadeh *et al.* 2015). The dislocation density is 1.96×10^{15} m^{-2} and 4.63×10^{15} m^{-2} for the NWs of MnO_2 and rGO/MnO_2, respectively. The results are summarized in Table 1.

To gain more structural information, the Raman spectra of MnO_2 and rGO/MnO_2 NWs are shown in Figure 1(b). Three core peaks at 506 cm^{-1}, 565 cm^{-1}, and 648 cm^{-1} are identified for the MnO_2 NWs. The Raman band at 648 cm^{-1} is due to the symmetric v_2 (Mn–O) stretching vibration of MnO_6 groups, and the band at 565 cm^{-1} is attributed to the v_3 (Mn–O) stretching vibration in the basal plane of MnO_6 sheets (Li *et al.* 2012). The low-frequency Raman band at 506 cm^{-1} refers to an external vibration that is due to the translational motion of the MnO_6 octahedra, thus revealing good crystallinity of the α-MnO_2. The rGO is characterized using the Raman spectrum by two specific peaks, G band at 1,599.4 cm^{-1} which is a characteristic of sp^2-hybridized C–C bonds in a two-dimensional hexagonal lattice, and D band at 1,345.8 cm^{-1} corresponding to the defects in the graphene structure. As shown in Figure 1(b), the I_D/I_G ratio is reduced slightly from 0.99 for rGO to 0.97 for rGO/MnO_2 NWs, due to the presence of defects during hydrothermal reduction. In addition, the characteristic band observed at 572.2 cm^{-1} in rGO/MnO_2 NWs belongs to A_g spectroscopic species originating from breathing vibrations of MnO_6 octahedral, suggesting the successful integration of MnO_2 into rGO (Yao *et al.* 2013).

Table 1 | The structural parameters of α-MnO_2 NWs and rGO/MnO_2 NWs

Sample	Crystallite size (nm)	Minimum dislocation density ($\times 10^{15}$ m^{-2})	Pore volume (cm^3 g^{-1})	Surface area (m^2 g^{-1})
MnO_2	22.54	1.96	0.020	37.7
rGO-MnO_2	14.69	4.63	0.032	59.1

Figure 2(a) shows scanning electron microscopy (SEM) images of MnO_2 NWs. The NWs shown in Figure 2(a) are small and attached to each other at the top of the view. From Figure 2(B-b), it is clear that the MnO_2 NWs grew on the surface of the GO sheets that acted as substrates for the nucleation of MnO_2 NWs, indicating that this is a heterogeneous nucleation. Furthermore, when there are more nucleation sites, it is expected to have more MnO_2 NWs with relatively thinner diameters, which is evident from the SEM images shown in Figure 2(a) compared to Figure 2(B-a), thus resulting in a higher surface area. The average surface area, from BET analysis, calculated for rGO/MnO_2 NWs is about 59.1 m^2 g^{-1}, whereas for pristine MnO_2 NW it is about 37.7 m^2 g^{-1}. The increased surface area of NWs is due to the presence of rGO nanosheets in the rGO/MnO_2. The graphene nanosheets were predominantly in the form of a few layers, with some single layer containing a number of pores. Therefore, the presence of rGO nanosheets in rGO/MnO_2 NWs cause more pore volume of around 0.032 cm^3 g^{-1} using BET analysis. By comparison for bare MnO_2 NWs the pore volume is 0.020 cm^3 g^{-1}, leading led to a greater surface area of rGO/MnO_2 NWs (Samejima *et al.* 1977, pp. 7–27). Evidently, the BET surface area of the rGO/MnO_2 NWs was found to be more than that of the bare MnO_2 NWs. This indicated that the MnO_2 NWs on the surface of rGO, as shown in both parts of Figure 2(b), possess an enhanced surface area.

The morphology of the rGO sheet is shown in the inset of Figure 2(B-a), revealing a crumpled structure after exfoliation (Kakaei & Hasanpour 2014). Therefore, from Raman and scanning electron microscopy studies, it is evident that MnO_2 NWs are wrapped with rGO sheets, which prevents the agglomeration of MnO_2 NWs. Figure 2(B-b) shows the rippled morphology of the rGO sheets, bundling MnO_2 NWs at lower magnification.

Catalysis: the Fenton and ultrasonic-combined Fenton process

The catalytic activity of the products was performed in a 250 mL borosil glass beaker. Initially, the reactants consisted of a 10 μM RB5 compound with 100 mL H_2O and pH was set at 5 using sulfuric acid or a sodium hydroxide solution. Subsequently, a 20 mg catalyst MnO_2 or rGO/MnO_2 was added to the solution. After mixing 6 mL of 30 wt% hydrogen peroxide solutions, O_2 bubbles were produced simultaneously. The resulting suspension was stirred on a magnetic stirrer for 30 min to attain the adsorption/desorption equilibrium between dye RB5 and suspended solid particles. In addition, an rGO/MnO_2 stock solution was

Downloaded from http://iwaponline.com/wst/article-pdf/76/7/1652/450029/wst076071652.pdf
by guest

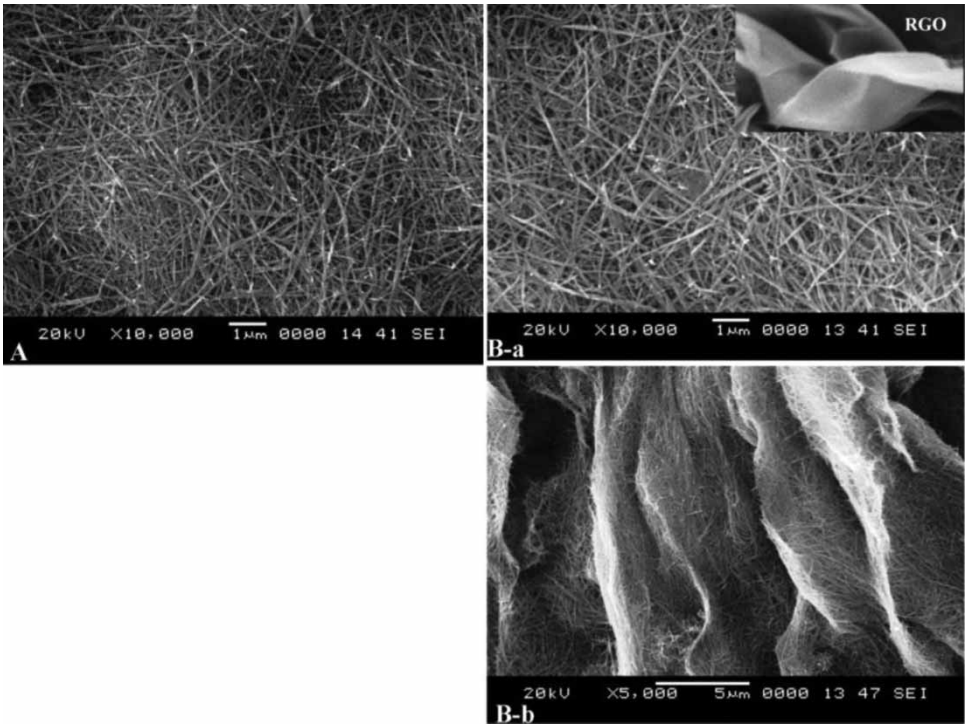

Figure 2 | Scanning electron microscopy images of: (A) MnO_2 NWs; (B–a) rGO/MnO_2 NWs; and (B-b) rGO/MnO_2 NWs at larger scale showing ripple like morphology due to graphene.

dispersed with probe sonication using an ultrasonic power of 120 W and a frequency of $20 + 2$ kHz. The tip of the probe was 6 cm in length, and 1 cm in diameter. pH was again tuned to a desired value at a reaction temperature of $40 \pm 2\ ^{\circ}C$. The ultrasonication facilitates a direct contact of the reaction matrix with the mechanical vibrations without significant loss of energy. Ultrasonic-combined Fenton experiments were carried out in a 50 mL polypropylene beaker at a regular time interval from 0 to 60 min. The samples designated as MnO_2, rGO/MnO_2, and US/rGO/MnO_2 were used for catalysis. After achieving the complete adsorption/desorption equilibrium state, the analytical samples (5 mL) were extracted from the solution at the regular time intervals. Subsequently, the catalyst was separated from the solution by centrifugation at 2,000 rpm for 10 min and the remaining solution was analyzed by an ultraviolet visible spectrophotometer to measure the absorbance of the dye solution.

To study the catalytic oxidation ability of the above α-MnO_2 NWs, the decomposition of RB5 with the assistance of hydrogen peroxide was preferred as a probe reaction. A blank cuvette filled with ultrapure water was used prior to each measurement.

Figure 3(a)–3(c) show the plot of absorption vs wavelength of RB5 based on the ultraviolet visible absorption spectra as a function of the catalytic reaction period for the various catalysts. A spectrum analysis was performed in the wavelength range from 400 to 700 nm. The intensity of the absorption at the highest peak is directly proportional to the concentration of RB5 in the solution, and is used to determine the percentage of dye removed from the solution over the course of the experiment. From the spectrum, the percentage of dye remaining in the suspension at different reaction times (0–60 min) was determined by measuring the maximum absorbance value at $\lambda_{max} = 596$ nm.

The optical spectra of the RB5 solution based on the absorbance vs wavelength along with the decolorization rate at different reaction periods is shown in Figure 3(a)–3(c).

The intensity of the maximum absorption peak of the RB5 reduced gradually with time. It can also be noted that the maximum wavelength of absorption was changed from 600 nm to 596 nm, 590.5 nm, and 582.5 nm after reaction durations of 10 min, 20 min, and 60 min, respectively. The blue shifts of the absorption wavelength revealed the catalytic decay of the RB5 (Weng *et al.* 2013). Eventually, the unique absorption peak became wide and weak in intensity, indicating the decolorization of RB5.

Figure 3(a)–3(c) show the absorption curves of RB5 solution. The plot at $t = 0$ is the initial dye solution (100 mL, 20 mg L^{-1}) after stirring magnetically for 30 min to achieve

Downloaded from http://iwaponline.com/wst/article-pdf/76/7/1652/450029/wst076071652.pdf
by guest

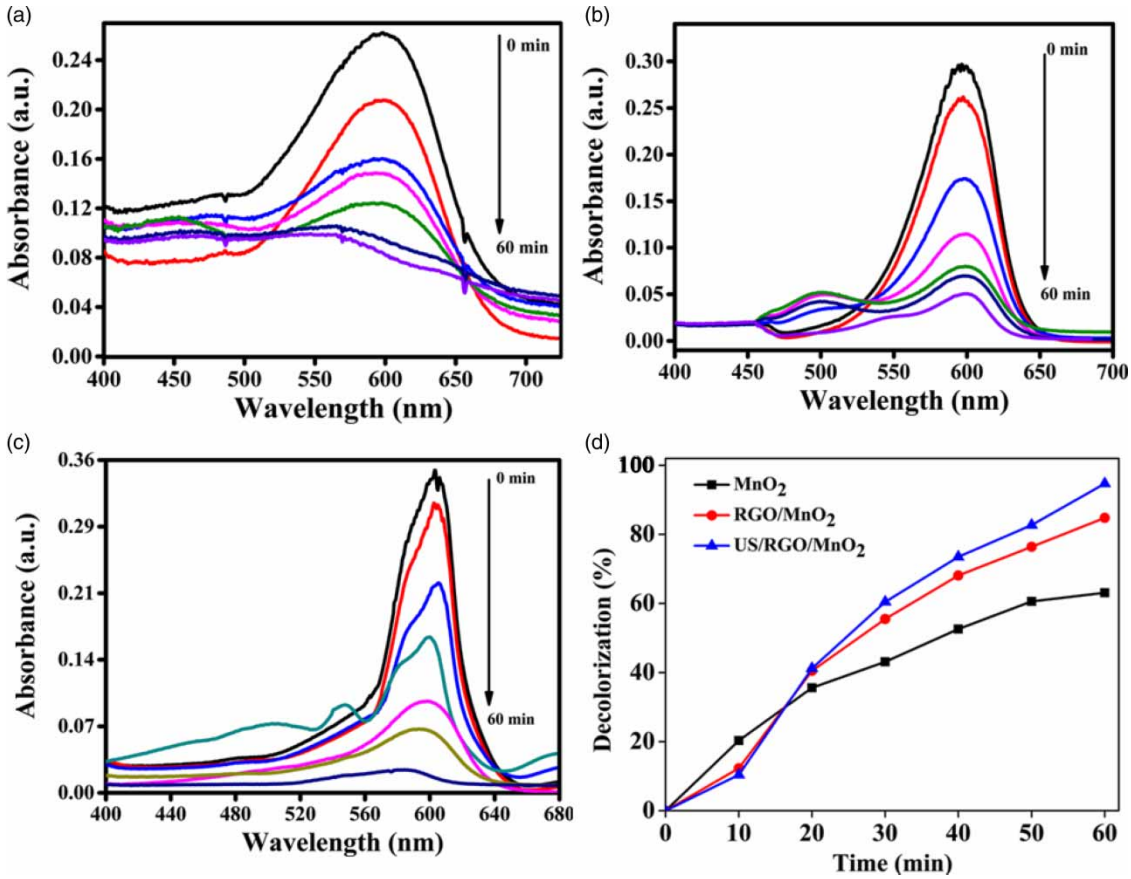

Figure 3 | The change in absorbance spectra of RB5 at different time intervals in the presence of (a) MnO_2 NWs, (b) rGO/MnO_2 NWs, and (c) US/rGO/MnO_2 NWs, and (d) the percentage decoloration of RB5 by MnO_2 NWs, rGO/MnO_2 NWs, and US/rGO/MnO_2 NWs as a function of time, revealing 63%, 84%, and 95% decoloration after 60 min, respectively. The concentration of the RB5 dye in the experiment is 10 μM and dosage of the materials (MnO_2 or rGO/MnO_2 (0.2 M of $MnSO_4$, 0.63 M of $KMnO_4$, and 0.025 gr of rGO)) is 20 mg.

adsorption/desorption equilibrium. Initially, a huge amount of dye is removed because of the larger generation of hydroxyl radicals accompanied by the fast disintegration of hydrogen peroxide. The concentration of dye in all samples decreases with increasing reaction time until the almost complete degradation of the dye.

Figure 3(d) shows the estimation of the degradation rate of RB5 by plotting decolorization (%) vs reaction time (t) for the three different catalysts. The color removal efficiency was estimated using the following expression,

$$Decolorization = \left(\frac{(C_0 - C_t)}{C_0}\right) \times 100 \quad (5)$$

where C_0 refers to the initial dye concentration, and C_t is the concentration of dye at time t (Chen *et al.* 2015). It may be noted that the use of US/rGO/MnO_2 as a catalyst resulted in the decolorization rate of 40% in only 20 min and as high as 95% in 60 min. In the same period, the highest effectiveness for dye elimination is 63% and 84% for MnO_2, and rGO/MnO_2, respectively.

We suggest the Fenton mechanism for the degradation of RB5. Briefly, the Fenton process uses the mixture of manganese ions and hydrogen peroxide to decay the pollutants via production of hydroxyl radicals in a catalytic process. Initially, hydrogen peroxide molecules could be adsorbed on the surface of rGO/MnO_2 NWs (Equation (6) in the Fenton reaction), then disintegrated into free radical species, such as $HO^{\bullet}$, O_2^{-} or $HOO^{\bullet}$ radical species, (Equations (7)–(10)). The generated free radical species ($HO^{\bullet}$, $O_2^{\bullet-}$) have the high oxidative capability to break the adsorbed dye molecules. Likewise, more RB5 molecules could transfer from the suspension to the MnO_2 surface and later be decayed into carbon dioxide, water and other small components, (Equation (11)). The obtained small components from the dye decomposition leave the catalyst surface by desorption, which results in recovery of a catalyst. Further, the hydrogen peroxide molecules in the Fenton

Downloaded from http://iwaponline.com/wst/article-pdf/76/7/1652/450029/wst076071652.pdf
by guest

reaction are mostly consumed in oxidizing the dye molecules and producing oxygen molecules with an assistance of free radical species (Equation (12)).

$$\mathrm{rGO/+\ or\ Mn(IV) + H_2O_2 \leftrightarrow rGO/+\ or\ Mn(IV)^{\bullet}H_2O_2} \quad (6)$$

$$\mathrm{rGO/+\ or\ Mn(IV)^{\bullet}H_2O_2 \rightarrow rGO/+\ or\ Mn(II) + HO_2^{\bullet} + H^+} \quad (7)$$

$$\mathrm{rGO/+\ or\ Mn(II) + H_2O_2 \rightarrow rGO + or\ Mn(IV) + HO^{\bullet} + OH^-} \quad (8)$$

$$\mathrm{HO_2^{\bullet} \leftrightarrow H^+ + O_2^{\bullet -}} \quad (9)$$

$$\mathrm{rGO/+\ orMnO_2 \bullet H_2O_2 \leftrightarrow HOO^- + H^+} \quad (10)$$

$$\mathrm{HO^{\bullet}(O_2^{\bullet -}) + dye(adsorbed) \rightarrow CO_2 + H_2O + \ldots.} \quad (11)$$

$$\mathrm{2HO^{\bullet} + 2HO^{\bullet} \rightarrow O_2 + 2H_2O} \quad (12)$$

The enhanced performance of rGO/MnO_2 towards the degradation of RB5 could be ascribed to the synergistic effect between MnO_2 and rGO in the presence of hydrogen peroxide. Graphene with 2D layers of sp^2-bonded structures can provide strong chemical and mechanical interactions, as well as increased electron transport between MnO_2 NWs and the rGO matrix (Qu *et al.* 2014). The RB5 molecules are easily adsorbed to the surfaces of GO through π–π conjugation based on its giant π-conjugation frame and two-dimensional planar configuration until the adsorption–desorption equilibrium. This accounts for the high concentration of hydroxyl radicals on the surface of rGO/MnO_2 NWs compared to bare MnO_2. Also, the structural and morphological properties of rGO/MnO_2 NWs reveal the superior catalytic activity.

Firstly, based on the XRD results, the average crystallite size of rGO/MnO_2 NWs is smaller with more dislocation density compare to the α-MnO_2 NWs. As a result of the lower particle size, the surface area increases, resulting in the adsorption of more H_2O_2 and dye molecules onto the surface of rGO/MnO_2. It is also evident from the BET data that the rGO/MnO_2 NWs reveals a higher surface area than the pristine MnO_2 NWs. This promotes the amount of reactive $^{\bullet}OH$ and $O_2^{\bullet -}$ free primitives attacking the dye molecules, leading to an enhancement in the degradation of RB5 molecules (Videla *et al.* 2015). Meanwhile, increased surface defects such as dislocations in the nanocomposite, as given in Table 1, play a crucial role in increasing the internal surface area of the catalyst, enhancing species diffusivity and chemical reactivity.

Secondly, it is evident from scanning electron microscopy analysis, that MnO_2 NWs are wrapped with rGO, which prevents the aggregation of MnO_2 NWs as well as serving as electron transfer channels to generate free radicals $^{\bullet}OH$, $HOO^{\bullet}$, or $O_2^{\bullet}$, which cause disintegration of RB5 molecules. As a result, the MnO_2/rGO NWs shows enhanced catalytic performance for degradation of RB5 dye.

To improve the degradation of RB5 further, we used ultrasonic treatment, where small size particles of rGO/MnO_2 catalyst were produced. In the ultrasonic-combined Fenton process, the collapse of the cavitation bubbles results in an extremely high temperature and pressure. These high-energy phenomena cause decomposition of organic effluents in aqueous solutions. The heat from the cavity collapse splits water molecules into abundantly reactive hydrogen and hydroxyl radicals (Equation (13)). The hydrogen radicals combine to create molecular hydrogen (H_2) and hydroxyl radicals combine to create hydrogen peroxide (Equations (14) and (15)). Meanwhile, hydrogen peroxide and O_2 molecules from the aqueous solution cause formation of oxide and other radicals (Equations (16 and 17)), where))))] indicates the ultrasound. $rGO/Mn\text{-}OOH^{2+}$ degenerate into Mn^{2+} and $^{\bullet}OOH$ (Equation (18)) due to a synergetic effect between Fenton's reagent and ultrasound. The separated Mn(II) ions can react ultimately with hydrogen peroxide to create hydroxyl radicals, leading to a cyclic process (Bagal & Gogate 2014). Therefore, the synergy of ultrasound and Fenton's process together increases the reaction rate of Mn^{2+} isolation from $Mn\text{-}OOH^{2+}$ and accelerates the hydroxyl radical formation due to the reaction between Mn^0/H_2O, Mn^{2+}/H_2O_2 or Mn^{3+}/H_2O, as shown in Equations (19)–(22). The generated hydroxyl radicals can react with RB5 molecules evolving carbon dioxide and water (Equation (23)).

$$\mathrm{H_2O +))) \leftrightarrow^{\bullet} OH + H^{\bullet}} \quad (13)$$

$$\mathrm{2H^{\bullet} \rightarrow H_2} \quad (14)$$

$$\mathrm{OH^{\bullet} + OH^{\bullet} \rightarrow H_2O_2} \quad (15)$$

$$\mathrm{H_2O_2 +))) \rightarrow 2^{\bullet}OH} \quad (16)$$

Downloaded from http://iwaponline.com/wst/article-pdf/76/7/1652/450029/wst076071652.pdf
by guest

$$O_2 +))) \rightarrow 2O^{\bullet} \quad (17)$$

$$rGO/Mn\text{-}OOH^{2+} +))) \rightarrow Mn^{2+} + HOO^{\bullet} \quad (18)$$

$$Mn^{2+} + H_2O_2 +))) \rightarrow Mn^{3+} + {}^{\bullet}OH + OH^{-} \quad (19)$$

$$Mn^{3+} + H_2O +))) \rightarrow Mn^{2+} + {}^{\bullet}OH + H^{+} \quad (20)$$

$$Mn^{0} + 2H_2O +))) \rightarrow Mn^{2+} + H_2 + 2{}^{\bullet}OH \quad (21)$$

$$2Mn^{0} + O_2 + 2H_2O +))) \rightarrow 2Mn^{2+} + 2H_2 + 4{}^{\bullet}OH \quad (22)$$

$$Dye + HO^{\bullet} \rightarrow [Dye\text{-}OH\,adduct]^{*} \rightarrow Oxidized dye + CO_2 + H_2O \quad (23)$$

As seen in Figure 3(d), after 60 min, the degradation efficiency in Fenton's process is 84.5%. However, during the same period, the ultrasonic-combined Fenton process results in about 95% decolorization. The results clearly indicate the significant enhancement in the ultrasonic-combined Fenton process compared with Fenton's alone could be due to the synergistic effects. The maximum color removal efficiency of RB5 in the present work is relatively more than the reported values, as shown in Table 2. rGO/MnO_2 NWs catalyst exhibits better performance in terms of low dosage and short reaction time and efficiency.

The decomposition yield formed at the end of the reaction for 60 min was examined by GC–MS and identified with mass spectra data for various catalysts (20 mg L^{-1} each) of RB5/MnO_2 (Figure 4(a)), RB5/rGO/MnO_2 (Figure 4(b)) and US/RB5/rGO/MnO_2 (Figure 4(c)).

It is evident from Figure 4 that the intensity of the corresponding peaks increases consistently from RB5/MnO_2, RB5/rGO/MnO_2, to US/RB5/rGO/MnO_2, indicating the higher decomposition rate of the dye by the ultrasonic-combined Fenton process. Particularly, the selected peaks at m/z ratio value 78, 106, 143, 198 and 300 match very well with the organic by-products as given in Table 3.

The various organic species after the disintegration of RB5 may have been formed through the following steps: (i) cleavage of the benzene ring; (ii) cleavage of the S–C bond between the aromatic ring and the sulfonate groups by the hydroxyl radicals attack; (iii) breaking of various N–C and C–C bonds of the chromophore compound, loss of sodium ions plus the gain of hydrogen; and (iv) –N = N– double bond split (Sharma & Roy 2015).

Table 2 | Reported values for decolorization of RB5 using MnO_2 and GO

Material	Method	Catalyst dose (mg)	RB5 dye concentration	Degradation (%)	Time (min)	Reference
α-MnO_2	Fenton	20	1×10^{-5} M	38	60	Ramesh *et al.* (2016)
Mn-alginate	Fenton	6,000	air flow 1 L/min	98	100	Fernández de Dios *et al.* (2015)
MnP	Biodegradation	20	25 mg/L	80	90	Mahmoudian *et al.* (2014)
GO	Fenton	300	1×10^{-5} M	57–75	5 h	Cheng *et al.* (2012)
Magnetic GO	Fenton	20	20 mL	62	60	Ali *et al.* (2014)
rGO	Photo catalytic	30	10 mg/L	26	60	Wong *et al.* (2015)
GO NPs	Fenton	1,000	1×10^{-5} M	80	2 h	Kyzas *et al.* (2014)
Fe alginate	Fenton	500	2.68 mM	85	60	Iglesias *et al.* (2013)
FO	Fenton	100	100 mg^{-1}	68	120	Meriç *et al.* (2004)
Fe	Fenton	300	50 mg^{-1}	63	120	Rahmani *et al.* (2010)
$FeSO_4$	Fenton	250	50 mg^{-1}	63	20	Lucas & Peres (2006)
NiO/Al_2O_3	Fenton	200	100 mg^{-1}	53	250	Bradu *et al.* (2010)
CuO/Al_2O_3/phosphate	Fenton	200	100 mg^{-1}	37.5	250	–
β-MnO_2	Fenton	160	40 mg^{-1}	56	40	Yu *et al.* (2014)
α-MnO_2	Fenton	20	1×10^{-5} M	63	60	Present work
rGO/α-MnO_2	Fenton	20	1×10^{-5} M	84	60	Present work
rGO/α-MnO_2	Sono-Fenton	20	1×10^{-5} M	95	60	Present work

Downloaded from http://iwaponline.com/wst/article-pdf/76/7/1652/450029/wst076071652.pdf
by guest

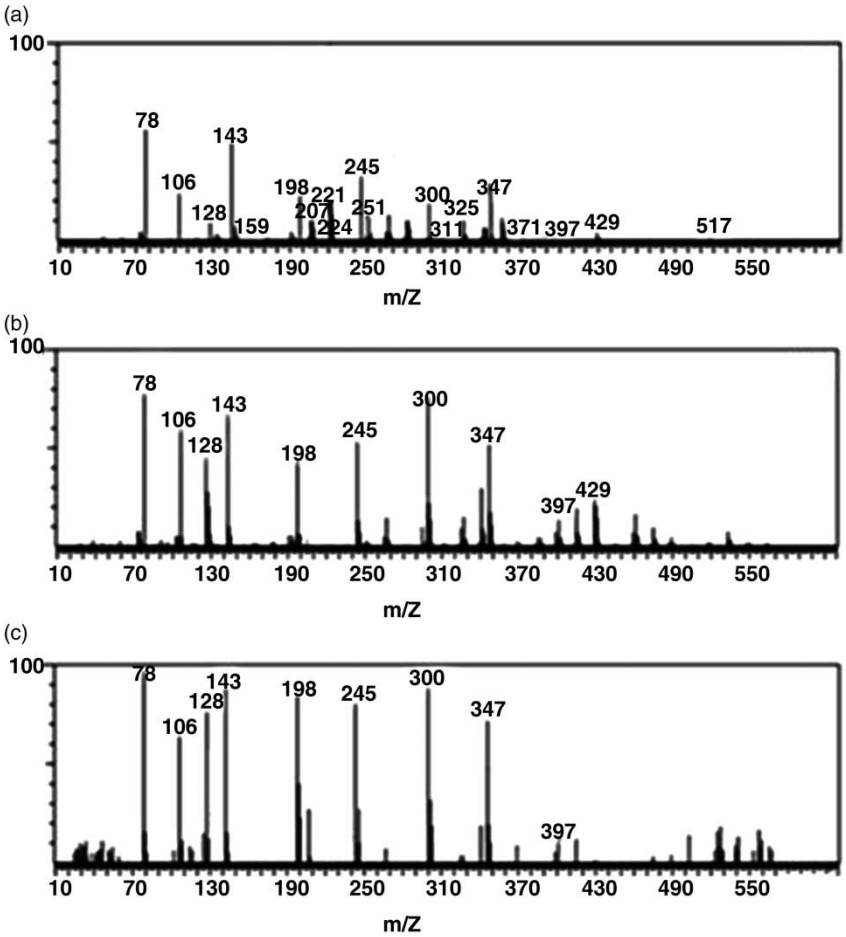

Figure 4 | Gas chromatography-mass spectrometry chromatograms obtained for decolorization of dye RB5 with the catalysts (a) MnO_2 NWs, (b) rGO/MnO_2 NWs, and (c) US/rGO/MnO_2 NWs observed after 60 min.

Effect of operational parameters

In order to determine the effect of other parameters on the decoloration of the pollutant, experiments were performed at constant pH = 5 for 60 min, using the ultrasonic-combined Fenton catalysis, with different concentrations of dye, rGO/MnO_2, and H_2O_2.

Effect of dye concentration

The concentration of dye is one of the main parameters in an ultrasonic-combined Fenton reaction. The decomposition of the dye was studied by varying the initial concentration range from 10 to 20 μM at pH = 5, with 20 mg catalyst rGO/MnO_2 NWs loading. The results are shown in Figure 5(a). As the concentration of the dye increases, the molecules bond strongly to the catalyst surface which then reduces the efficiency of the catalytic reaction due to the decline in $OH^{\cdot}$ and $OH_2^{\cdot}$ concentrations, leading to saturation and a lower degradation rate. Also, the existence of a large amount of adsorbed dye decreases the probability of direct contact with the hydroxyl radicals, resulting in an inhibitive effect on the dye degradation (Tayeb & Hussein 2015).

Effect of catalyst amount

The amount of catalyst in the ultrasonic-combined Fenton reaction is another factor taken into consideration. Generally it is observed that the percentage degradation increases when increasing the amount of catalyst, while keeping other factors fixed. As the catalyst amount increases, a larger quantity of dye is adsorbed on the surface of the rGO/MnO_2 NWs. This increases the probability of a reaction between dye molecules and oxidizing species, thus causing an enhancement in the degradation percentage

Downloaded from http://iwaponline.com/wst/article-pdf/76/7/1652/450029/wst076071652.pdf
by guest

Table 3 | Possible degradation products of RB5 after catalytic reaction as determined using GC–MS

Intermediates formed during degradation of RB-5	Name of the intermediate
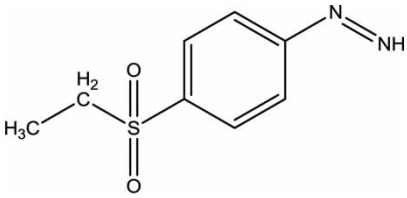	(4-ethylsulfonyl)phenyl)diazene
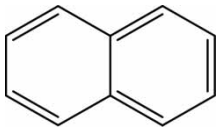	Naphthalene
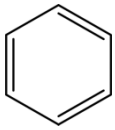	Benzene
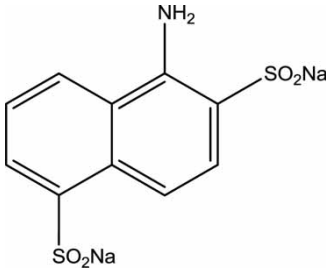	Sodium 5-aminonaphthalene-1,6-disulfinate
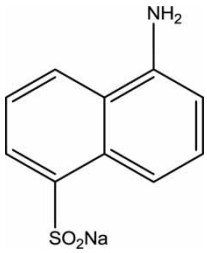	Sodium 5-aminonaphthalene-1-sulfinate
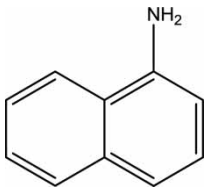	Naphthalen-1-amine
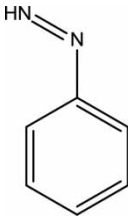	Phenyldiazene
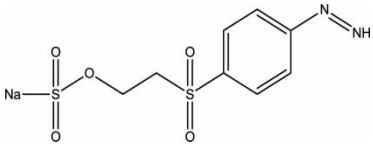	Sodium 1-[(4-sulfamoylphenyl)amino] ethanesulfonate

Downloaded from http://iwaponline.com/wst/article-pdf/76/7/1652/450029/wst076071652.pdf
by guest

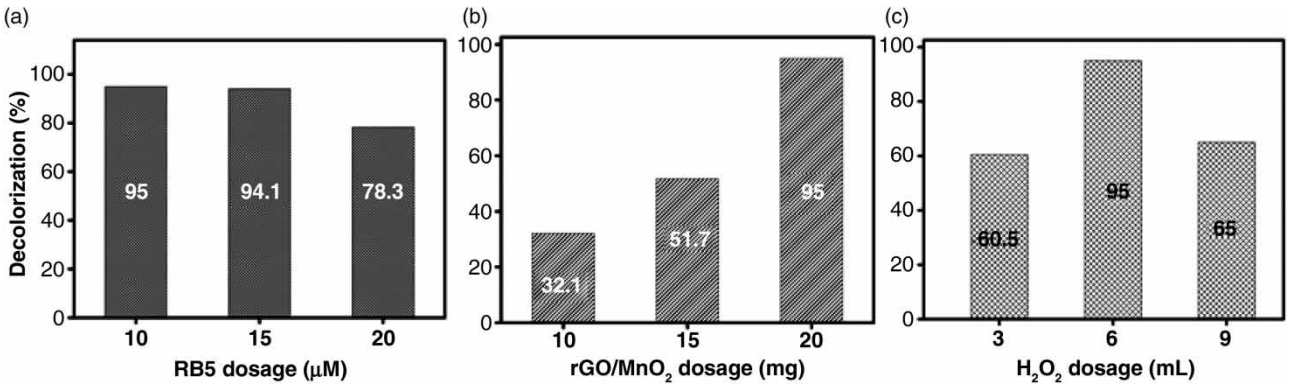

Figure 5 | Effect of variation in the dosage of (a) dye, (b) catalyst, and (c) H_2O_2 on the decolorization of RB5 dye in the ultrasonic-combined Fenton reaction at pH 5 for a period of 60 min.

(Akpan & Hameed 2009). Figure 5(b) shows the affect of catalyst amount on the dye decolorization percentage.

Effect of H_2O_2 dosage

The ultrasonic-combined Fenton degradation of RB5 is also affected by the concentration of hydrogen peroxide in the solution. To determine the optimal dosage of the H_2O_2, 3–9 mL was mixed in the 100 mL dye solution. The degradation increased considerably when increasing the initial H_2O_2 concentration from 3 to 6 mL as shown in Figure 5(c). This is attributed to an increase in the adsorption and interfacial reactions, which in turn increases the number of hydroxyl radicals. As the concentration of H_2O_2 is further increased from 6 to 9 mL, the solution becomes turbid and blocks the Fenton reaction, and therefore the percentage degradation of the dye decreased (Alaton & Balcioglu 2001). However, H_2O_2 itself acts as an effective $OH^{\bullet}$ scavenger at concentrations that are specific for the pollutant, according to the empirical equation

$$H_2O_2 + OH^{\bullet} \rightarrow HO_2^{\bullet} + H_2O.$$

Thus, the presence of excess H_2O_2 can lower the treatment efficiency of the Fenton reaction.

The cyclic life of the prepared MnO_2 NWs, rGO/MnO_2 NWs was also studied using the degradation of the RB5 as shown in Figure 6. In order to check the reusability of MnO_2 NWs, they were filtered, washed with deionized water and dried in air at 60 °C for 4 h, and reused in the number of cycles from the Ist to Vth cycle. The degradation efficiency reduces slightly from 84.5% to 81.2% for GO/MnO_2 NWs, whereas, the degradation efficiency largely reduced from 63.1% to 55.5% in the case of pristine MnO_2

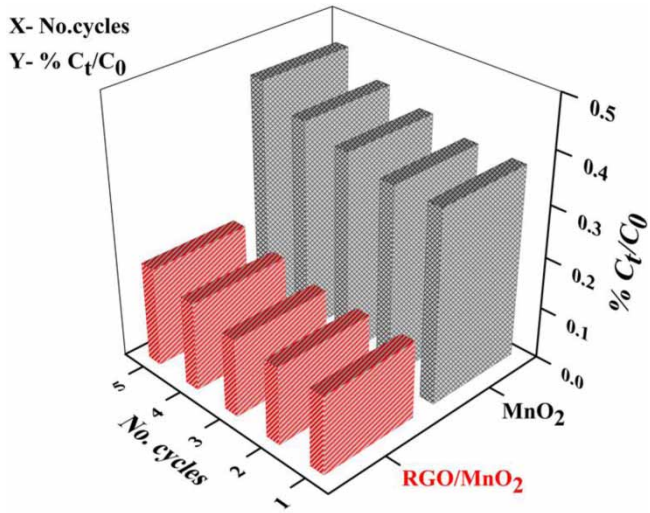

Figure 6 | Recycling (5 cycles) performance of the α-MnO_2 NWs and rGO/MnO_2 NWs for the degradation of the RB5 after 60 min.

NWs, because some amount of catalyst is lost during centrifugation, washing and filtration. The wrapping of MnO_2 NWs with rGO sheets reduces the contact of NWs during centrifugation, as well as their solubility in water. This is attributed to the lower mass loss of the rGO/MnO_2 NWs compared with the pristine MnO_2 NWs. Therefore, rGO/MnO_2 NWs have cyclic stability and can be reprocessed without substantial reduction in catalytic performance for degradation of the RB5 in water.

CONCLUSIONS

MnO_2 NWs and rGO/MnO_2 NWs were synthesized by a simple hydrothermal method, and catalytic performance was tested using RB5 as a model pollutant. rGO/MnO_2

Downloaded from http://iwaponline.com/wst/article-pdf/76/7/1652/450029/wst076071652.pdf
by guest

NWs reveal superior catalytic performance towards the decomposition of the RB5, because the large surface area of sp^2-bonded rGO structure provides good electron transfer channels and interface dislocations. Besides, as has been shown by X-ray diffraction and scanning electron microscopy studies, the structural and morphological properties of NWs, such as defect density and agglomeration, are well correlated with the catalytic performance. The rGO coating of MnO_2 NWs results in 20% enhancement in catalytic activity compared to pristine MnO_2 NWs towards degradation of RB5 dye with hydrogen peroxide based on the Fenton catalysis. The application of a coupled ultrasonic-combined Fenton process using an rGO/MnO_2 catalyst, further enhances the degradation rate of RB5 by 30% due to synergic effects. Additionally, the as-grown rGO/MnO_2 retained its catalytic stability for several cycles due to the wrapping of NWs with rGO. The various intermediate byproducts formed during the catalytic reaction were successfully detected with higher production rates in the ultrasonic-combined Fenton reaction compared to the Fenton reaction. Therefore, rGO/MnO_2 NWs exhibit good catalytic activity and can be used for environmental protection.

ACKNOWLEDGEMENTS

H. S. Nagaraja acknowledges the Government of India for financial support through the DST-SERB project (No. SB/S2/CMP-105/2013).

REFERENCES

Abdolhosseinzadeh, S., Asgharzadeh, H. & Kim, H. S. 2015 Fast and fully-scalable synthesis of reduced graphene oxide. *Scientific Reports* **5**, 10160.

Aguedach, A., Brosillon, S., Morvan, J. & Lhadi, E. K. 2008 Influence of ionic strength in the adsorption and during photocatalysis of Reactive Black 5 azo dye on TiO_2 coated on non-woven paper with SiO_2 as a binder. *Journal of Hazardous Materials* **150**, 250–256.

Ai, Z., Zhang, L., Kong, F., Liu, H., Xing, W. & Qiu, J. 2008 Microwave-assisted green synthesis of MnO_2 nanoplates with environmental catalytic activity. *Materials Chemistry and Physics* **111**, 162–167.

Akpan, U. G. & Hameed, B. H. 2009 Parameters affecting the photocatalytic degradation of dyes using TiO_2-based photocatalysts: a review. *Journal of Hazardous Materials* **170**, 520–529.

Alaton, I. A. & Balcioglu, I. A. 2001 Photochemical and heterogeneous photocatalytic degradation of waste vinylsulphone dyes: a case study with hydrolyzed Reactive Black 5. *Journal of Photochemistry and Photobiology A: Chemistry* **141**, 247–254.

Ali, L., Alhassani, H., Karuvantevida, N., Rauf, M. A. & Ashraf, S. S. 2014 Efficient aerobic degradation of various azo dyes by a *Sphingomonas* sp. isolated from petroleum sludge. *Journal of Bioremediation & Biodegradation* **5**, 1.

Amin, M. T., Alazba, A. A. & Shafiq, M. 2015 Adsorptive removal of Reactive Black 5 from wastewater using bentonite clay: isotherms, kinetics and thermodynamics. *Sustainability* **7**, 15302–15318.

Bagal, M. V. & Gogate, P. R. 2014 Wastewater treatment using hybrid treatment schemes based on cavitation and Fenton chemistry: a review. *Ultrasonics Sonochemistry* **21**, 1–14.

Basturk, E. & Karatas, M. 2014 Advanced oxidation of Reactive Blue 181 solution: a comparison between Fenton and sono-Fenton process. *Ultrasonics Sonochemistry* **21**, 1881–1885.

Bradu, C., Frunza, L., Mihalche, N., Avramescu, S.-M., Neaţă, M. & Udrea, I. 2010 Removal of Reactive Black 5 azo dye from aqueous solutions by catalytic oxidation using CuO/Al_2O_3 and NiO/Al_2O_3. *Applied Catalysis B: Environmental* **96**, 548–556.

Chen, W., Zheng, L., Jia, R. & Wang, N. 2015 Cloning and expression of a new manganese peroxidase from *Irpex lacteus* F17 and its application in decolorization of Reactive Black 5. *Process Biochemistry* **50**, 1748–1759.

Chen, X., Dai, J., Shi, G., Li, L., Wang, G. & Yang, H. 2016 Sonocatalytic degradation of Rhodamine B catalyzed by β-Bi_2O_3 particles under ultrasonic irradiation. *Ultrasonics Sonochemistry* **29**, 172–177.

Cheng, J.-S., Du, J. & Zhu, W. 2012 Facile synthesis of three-dimensional chitosan–graphene mesostructures for Reactive Black 5 removal. *Carbohydrate Polymers* **88**, 61–67.

Chong, M. N., Cho, Y. J., Poh, P. E. & Jin, B. 2015 Evaluation of titanium dioxide photocatalytic technology for the treatment of Reactive Black 5 dye in synthetic and real greywater effluents. *Journal of Cleaner Production* **89**, 196–202.

Feng, X., Yan, Z., Chen, N., Zhang, Y., Ma, Y., Liu, X., Fan, Q., Wang, L. & Huang, W. 2013 The synthesis of shape-controlled MnO_2/graphene composites via a facile one-step hydrothermal method and their application in supercapacitors. *Journal of Materials Chemistry A* **1**, 12818–12825.

Fernández de Dios, M., Á., Rosales, E., Fernández, M., F., Pazos, M. & Sanromán, M., Á. 2015 Degradation of organic pollutants by heterogeneous electro Fenton process using Mn-alginate-composite. *Journal of Chemical Technology and Biotechnology* **90**, 1439–1447.

Fu, C., Zhao, G., Zhang, H. & Li, S. 2013 Evaluation and characterization of reduced graphene oxide nanosheets as anode materials for lithium-ion batteries. *Int. J. Electrochem. Sci.* **8**, 6269–6280.

Gupta, V. K., Ali, I., Saleh, T. A., Nayak, A. & Agarwal, S. 2012 Chemical treatment technologies for waste-water recycling: an overview. *RSC Advances* **2**, 6380–6388.

Downloaded from http://iwaponline.com/wst/article-pdf/76/7/1652/450029/wst076071652.pdf
by guest

Harichandran, G. & Prasad, S. 2016 Sonofenton degradation of an azo dye, Direct Red. *Ultrasonics Sonochemistry* **29**, 178–185.

Iglesias, O., De Dios, M. F., Rosales, E., Pazos, M. & Sanromán, M. A. 2013 Optimisation of decolourisation and degradation of Reactive Black 5 dye under electro-Fenton process using Fe alginate gel beads. *Environmental Science and Pollution Research* **20**, 2172–2183.

Kakaei, K. & Hasanpour, K. 2014 Synthesis of graphene oxide nanosheets by electrochemical exfoliation of graphite in cetyltrimethylammonium bromide and its application for oxygen reduction. *Journal of Materials Chemistry A* **2**, 15428–15436.

Kalkan, E., Nadaroğlu, H., Celebi, N. & Tozsin, G. 2014 Removal of textile dye Reactive Black 5 from aqueous solution by adsorption on laccase-modified silica fume. *Desalination and Water Treatment* **52**, 6122–6134.

Kansal, S. K., Kaur, N. & Singh, S. 2009 Photocatalytic degradation of two commercial reactive dyes in aqueous phase using nanophotocatalysts. *Nanoscale Research Letters* **4**, 709.

Karatas, M., Argun, Y. A. & Argun, M. E. 2012 Decolorization of antraquinonic dye, Reactive Blue 114 from synthetic wastewater by Fenton process: kinetics and thermodynamics. *Journal of Industrial and Engineering Chemistry* **18**, 1058–1062.

Kumar, B. P., Shivaprasad, K. H., Raveendra, R. S., Hari Krishna, R., Karikkat, S. & Nagabhushana, B. M. 2014 Preparation of MnO_2 nanoparticles for the adsorption of environmentally hazardous malachite green dye. *Int. J. Appl. Innov. Eng. Manag.* **3**, 102–106.

Kyzas, G. Z., Deliyanni, E. A. & Matis, K. A. 2014 Graphene oxide and its application as an adsorbent for wastewater treatment. *Journal of Chemical Technology and Biotechnology* **89**, 196–205.

Li, Z., Ding, Y., Xiong, Y. & Xie, Y. 2005 Rational growth of various α-MnO_2 hierarchical structures and β-MnO_2 nanorods via a homogeneous catalytic route. *Crystal Growth & Design* **5**, 1953–1958.

Li, Y., Wang, J., Zhang, Y., Banis, M. N., Liu, J., Geng, D., Li, R. & Sun, X. 2012 Facile controlled synthesis and growth mechanisms of flower-like and tubular MnO_2 nanostructures by microwave-assisted hydrothermal method. *Journal of Colloid and Interface Science* **369**, 123–128.

Lucas, M. S. & Peres, J. A. 2006 Decolorization of the azo dye Reactive Black 5 by Fenton and photo-Fenton oxidation. *Dyes and Pigments* **71**, 236–244.

Mahmoudian, M. R., Alias, Y., Basirun, W. J., Woi, P. M. & Sookhakian, M. 2014 Facile preparation of MnO_2 nanotubes/reduced graphene oxide nanocomposite for electrochemical sensing of hydrogen peroxide. *Sensors and Actuators B: Chemical* **201**, 526–534.

Meriç, S., Kaptan, D. & Ölmez, T. 2004 Color and COD removal from wastewater containing Reactive Black 5 using Fenton's oxidation process. *Chemosphere* **54**, 435–441.

Namkung, K.-C., Burgess, A. E., Bremner, D. H. & Staines, H. 2008 Advanced Fenton processing of aqueous phenol solutions: a continuous system study including sonication effects. *Ultrasonics Sonochemistry* **15**, 171–176.

Peng, L., Peng, X., Liu, B., Wu, C., Xie, Y. & Yu, G. 2013 Ultrathin two-dimensional MnO_2/graphene hybrid nanostructures for high-performance, flexible planar supercapacitors. *Nano Letters* **13**, 2151–2157.

Poulios, I. & Tsachpinis, I. 1999 Photodegradation of the textile dye Reactive Black 5 in the presence of semiconducting oxides. *Journal of Chemical Technology and Biotechnology* **74**, 349–357.

Qu, J., Shi, L., He, C., Gao, F., Li, B., Zhou, Q., Hu, H., Shao, G., Wang, X. & Qiu, J. 2014 Highly efficient synthesis of graphene/MnO_2 hybrids and their application for ultrafast oxidative decomposition of methylene blue. *Carbon* **66**, 485–492.

Rahmani, A. R., Zarrabi, M., Samarghandi, M. R., Afkhami, A. & Ghaffari, H. R. 2010 Degradation of azo dye Reactive Black 5 and Acid Orange 7 by Fenton-like mechanism. *Iranian Journal of Chemical Engineering* **7**, 87–94.

Ramesh, M., Nagaraja, H. S., Rao, M. P., Anandan, S. & Huang, N. M. 2016 Fabrication, characterization and catalytic activity of α-MnO_2 nanowires for dye degradation of Reactive Black 5. *Materials Letters* **172**, 85–89.

Sadeghi, A., Bazardehi, M. A. K., Raffe, S. & Zarif, B. 2014 Biotransformation of Carmoisine and Reactive Black 5 dyes using *Saccharomyces cerevisiae*. *Health* **6**, 859.

Samejima, T., Yoshihiko, S. O. H. & Toshimasa, Y. 1977 Specific surface area and specific pore volume distribution of tobacco. *Agricultural and Biological Chemistry* **41**, 983–988.

Sharma, S. & Roy, S. 2015 Biodegradation of dye Reactive Black 5 by a novel bacterial endophyte. *International Research Journal of Environmental Sciences* **4**, 44–53.

Siboni, M. S., Samarghandi, M., Yang, J.-K. & Lee, S.-M. 2011 Photocatalytic removal of Reactive Black 5 dye from aqueous solution by UV irradiation in aqueous TiO_2: equilibrium and kinetics study. *Journal of Advanced Oxidation Technologies* **14**, 302–307.

Siddique, M., Farooq, R. & Price, G. J. 2014 Synergistic effects of combining ultrasound with the Fenton process in the degradation of Reactive Blue 19. *Ultrasonics Sonochemistry* **21**, 1206–1212.

Song, Y.-L., Li, J.-T. & Chen, H. 2009 Degradation of CI Acid Red 88 aqueous solution by combination of Fenton's reagent and ultrasound irradiation. *Journal of Chemical Technology and Biotechnology* **84**, 578–583.

Sreejesh, M., Huang, N. M. & Nagaraja, H. S. 2015 Solar exfoliated graphene and its application in supercapacitors and electrochemical H_2O_2 sensing. *Electrochimica Acta* **160**, 94–99.

Tayeb, A. M. & Hussein, D. S. 2015 Synthesis of TiO_2 nanoparticles and their photocatalytic activity for Methylene Blue. *American Journal of Nanomaterials* **3**, 57–63.

Videla, A. H., Osmieri, L., Esfahani, R. A. M., Zeng, J., Francia, C. & Specchia, S. 2015 The use of C-MnO_2 as hybrid precursor support for a Pt/C-Mn_xO_{1+x} catalyst with enhanced activity for the methanol oxidation reaction (MOR). *Catalysts* **5**, 1399–1416.

Downloaded from http://iwaponline.com/wst/article-pdf/76/7/1652/450029/wst076071652.pdf
by guest

Vijayaraghavan, J., Basha, S. S. & Jegan, J. 2013 A review on efficacious methods to decolorize reactive azo dye. *Journal of Urban and Environmental Engineering (JUEE)* **7**. http://periodicos.ufpb.br/ojs2/index.php/juee/article/view/12733 (accessed 6 April 2017).

Weng, C.-H., Lin, Y.-T. & Yuan, H.-M. 2013 Rapid decoloration of Reactive Black 5 by an advanced Fenton process in conjunction with ultrasound. *Separation and Purification Technology* **117**, 75–82.

Williamson, G. K. & Smallman, R. E. 1956 III. Dislocation densities in some annealed and cold-worked metals from measurements on the X-ray Debye-Scherrer spectrum. *Philosophical Magazine* **1**, 34–46.

Wong, C. P. P., Lai, C. W., Lee, K. M. & Hamid, S. B. A. 2015 Advanced chemical reduction of reduced graphene oxide and its photocatalytic activity in degrading Reactive Black 5. *Materials* **8**, 7118–7128.

Wu, Y., Lu, Y., Song, C., Ma, Z., Xing, S. & Gao, Y. 2013 A novel redox-precipitation method for the preparation of α-MnO_2 with a high surface Mn^{4+} concentration and its activity toward complete catalytic oxidation of *O*-xylene. *Catalysis Today* **201**, 32–39.

Yao, Y., Xu, C., Yu, S., Zhang, D. & Wang, S. 2013 Facile synthesis of $Mn_3O_4^-$ reduced graphene oxide hybrids for catalytic decomposition of aqueous organics. *Industrial & Engineering Chemistry Research* **52**, 3637–3645.

Yu, C., Li, G., Wei, L., Fan, Q., Shu, Q. & Jimmy, C. Y. 2014 Fabrication, characterization of β-MnO_2 microrod catalysts and their performance in rapid degradation of dyes of high concentration. *Catalysis Today* **224**, 154–162.

Zang, Z. & Tang, X. 2015 Enhanced fluorescence imaging performance of hydrophobic colloidal ZnO nanoparticles by a facile method. *Journal of Alloys and Compounds* **619**, 98–101.

Zhang, H., Zhang, D. & Zhou, J. 2006 Removal of COD from landfill leachate by electro-Fenton method. *Journal of Hazardous Materials* **135**, 106–111.

Zhang, Y. X., Guo, X. L., Huang, M., Hao, X. D., Yuan, Y. & Hua, C. 2015 Engineering birnessite-type MnO_2 nanosheets on fiberglass for pH-dependent degradation of Methylene Blue. *Journal of Physics and Chemistry of Solids* **83**, 40–46.

Zhong, N. 2016 Facile synthesis of MnO_2 nanoparticles well dispersed on graphene for the enhanced electrochemical performance. *Int. J. Electrochem. Sci.* **11**, 2525–2533.

First received 16 February 2017; accepted in revised form 4 May 2017. Available online 7 June 2017

Downloaded from http://iwaponline.com/wst/article-pdf/76/7/1652/450029/wst076071652.pdf
by guest